As has been discussed above, large enhancements were observed on 11/12 April and 17/18 May 2006 for the moderate earthquakes that occurred on 17 April and 21 May 2006. These enhancements were many times larger (about 115 and 48 times respectively) than the background for the respective months. On the basis of polarization ratios and also due to the use of night-time data, we conclude that these observed enhancements are, perhaps, seismogenic. Moreover, during these periods the geomagnetic activity was also low.

In the present case, we could observe large and convincing enhancements in magnetic-field intensities, 3–5 days before the occurrence of moderate, and nearby, earthquakes. This suggests that these enhancements can be treated as precursory signatures of the impending earthquakes. This may lead to short-term prediction of earthquakes.

However, we suggest that before establishing this technique beyond doubt, similar exercise may be undertaken on the basis of large database of moderate and strong earthquakes that might have occurred with nearby and distant epicentres.


1. Hayakawa, M., Hattori, K. and Ohta, K., Monitoring of ULF geomagnetic variations associated with earthquakes. *Sensors*, 2007, **7**, 1108–1122.
2. Koptenko, Y., Ismagilov, V., Hayakawa, M., Smirnova, N., Troyan, V. and Peterson, T., Investigation of the ULF electromagnetic phenomena related to earthquakes: Contemporary achievement and the perspective. *Ann. Geofis.*, 2001, **44**, 325–334.
3. Hayakawa, M., Kawate, R., Molchanov, O. A. and Kiyohumi, Y., Results of ultra-low-frequency magnetic field measurements during the Guam earthquake of 8 August 1993. *Geophys. Res. Lett.*, 1996, **23**, 241–244.
4. Faser-Smith, A. C., McGill, P. R., Helliwell, R. A. and Villard Jr O. G., Ultralow–frequency magnetic field measurements in southern California during the Northridge earthquake of January. *Geophys. Res. Lett.*, 1994, **21**, 2195–2198.
5. Hayakawa, M., Ito, T., Hattori, K. and Yumoto, K., ULF electromagnetic precursors for an earthquake at Biak, Indonesia on 17 February 1996. *Geophys. Res. Lett.*, 1996, **27**, 1531–1534.
6. Molachanov, O. A. and Hayakawa, M., Generation of ULF electromagnetic emission by microfacturing. *Geophys. Res. Lett.*, 1995, **22**, 3091–3094.
7. Bhattacharya, S., Shrivastava, A. and Gwal, A. K., Ground-based methodology for determining ultra low frequency (ULF) electromagnetic emissions associated with seismic activity. In IAGA WG1.2 on Electromagnetic Induction in the Earth Proceedings of the 17th Workshop, Hyderabad, India, 2004.
8. Eftaxias, K., Kapiris, P., Olygiannakis, J., Peratzakis, A., Kopanas, J., Antonopoulos, G. and Rigas, D., Experience of short term earthquake precursors with VLF–VHF electromagnetic emissions. *Nat. Hazards Earth Syst. Sci.*, 2003, **3**, 201–228.
9. Parrot, M., The micro-satellite DEMETER. *J. Geodyn.*, 2002, **33**, 535–541.
10. Kushwah, V., Vikram Singh, Birbal Singh and Hayakawa, M., Ultralow frequency (ULF) magnetic field anomalies observed at Agra and their relation to moderate seismic activities in Indian region. *J. Atmos. Sol.-Terr. Phys.*, 2005, **67**, 992–1001.
11. Hayakawa, M., Ohta, K., Nickolaenko, A. P. and Ando, Y., Anomalous effect in Schumann resonance phenomena observed in Japan, possibly associated with the Chi-chi earthquake in Taiwan. *Ann. Geophys.*, 2005, **23**, 1335–1346.
12. Hattori, K., Akinaga, Y., Hayakawa, M., Yumoto, K., Nagao, T. and Uyeda, S., ULF magnetic anomaly preceding the 1997 Kagoshima earthquakes. In *Seismo Electromagnetics: Lithosphere–Atmosphere–Ionosphere Coupling* (eds Hayakawa, M. and Molchanov, O. A.), Terr. Sc. Publ., Tokyo, 2002, pp. 19–28.


ACKNOWLEDGEMENTS. We thank the Department of Science and Technology, New Delhi for providing financial support through a project. Thanks are due to Dr R. S. Vhatkar and P. T. Patil for help during installation of the system. We also thank the referees for useful comments to revise the manuscript.

Received 19 February 2007; revised accepted 26 February 2008

# Extreme rainfall events: Vulnerability analysis for disaster management and observation system design

**P. Goswami* and K. V. Ramesh**

CSIR Centre for Mathematical Modelling and Computer Simulation, Wind Tunnel Road, Bangalore 560 037, India

**Extreme rainfall events today pose a serious threat to many populated and urbanized areas worldwide. An accurate estimate of frequency and distribution of these events can significantly aid in policy planning and observation system design. We report here a high-resolution (10 km) analysis of heavy rainfall episodes (defined as 24-h rainfall exceeding 250 mm) over the Indian region. The dataset, recently developed by NOAA, USA, provides daily composite rainfalls for the period 2001–06 at locations approximately 10 km apart. We first assess the reliability of the dataset by comparing it with daily gridded (1° × 1°) rainfall data from IMD and three-hourly gridded (0.25° × 0.25°) data from TRMM for the overlap years (2001–04). A category-wise analysis of the high-resolution data reveals a number of hotspots of vulnerability; in particular, the semiarid region in northwest India emerges as a high-vulnerability area in terms of extreme rainfall events. The high-resolution analysis also clearly reveals the corridor of the monsoon trough, lined by a flower-pot distribution of extreme rainfall events along the flanks. This can be a valuable input for precision design of field experiments on the continental trough or on localized extreme events like thunderstorms. Other important implications for areas like vulnerability assessment, planning and mesoscale forecasting are discussed.**

**Keywords:** Disaster management, extreme rainfall events, forecasting, vulnerability analysis.

*For correspondence. (e-mail: goswami@cmmacs.ernet.in)

THE last few decades have seen rapid, large-scale and often unplanned urbanization in many parts of the world, especially in India. More than 60% of the world population is projected to be urban by 2020, with India poised to develop a number of mega cities[1–3]. A serious consequence of such urbanization, and associated land use, is anticipated to be enhanced susceptibility and vulnerability of the urban population to high-impact weather events like episodes of intense rainfall, especially for high-density cities like those in South Asia. An example is the heavy rainfall event of 26–27 July 2005 over Mumbai, India, which alone caused a loss of more than 1500 lives and considerable loss of property. Vulnerability and agricultural sustainability are primarily local issues, and depend critically on the amount and temporal distribution of rainfall received over a region. Thus rainfall patterns need to be examined in a local perspective.

Applications like proactive disaster management and observation system design, however, require inputs at resolution, precision and accuracy not provided by isolated and sporadic measurements. Model forecasts can be valuable, and sometimes the only tool for generating information that goes into design and (proactive) response. However, for such forecasts to be effective, the models need to have proven (statistical) skill at required temporal and spatial resolutions. Similarly, quantitative estimates of the geographical distribution of vulnerability as well as reliable projection of future changes in the frequency, intensity and distribution of extreme rainfall events (hereafter ERE) require detailed observational inputs and other constraints. Such observational features of ERE with high spatio-temporal resolution were unavailable until recently, especially for the Indian region. While there now exists a long-period (1951–2004), daily gridded rainfall dataset over India due to an initiative by the India Meteorological Department (IMD), the resolution of this data ($1° \times 1°$) is too coarse to properly capture the highly localized ERE; in particular, if the ERE are found to be localized also in terms of occurrence, an analysis of much higher resolution is needed. Although there have been several studies on the occurrence and distribution of rainfall events over India[4], these have been primarily based on isolated station data and thus do not provide a large-scale picture[5,6].

Recently, beginning 1 May 2001, the Climate Prediction Center (CPC) of the National Oceanographic and Atmospheric Administration (NOAA), USA initiated a project to produce real-time analyses of daily precipitation on a 0.1° latitude/longitude grid over South Asia (70°E–110°E; 5°N–35°N). The inputs include GTS station data as well as geostationary infrared cloud-top temperature fields and polar orbiting satellite precipitation estimates from SSM/I and AMSU-B microwave sensors. Analysis of daily precipitation was generated by merging four kinds of observation-based individual datasets using the algorithm of Xie and Arkin[7,8]. Since events of high intensity considered here are rarely revealed by coarse-resolution datasets like NCEP Reanalysis (~250 km resolution)[9] or even the $1° \times 1°$ gridded daily rainfall recently prepared by IMD[10], we do not consider these datasets for analysis of ERE.

While we do not use the coarse-resolution ($1° \times 1°$) IMD data for analysing ERE, we use it to ensure reliability of the relatively less tested high-resolution rainfall (HRR) data. We examine this issue for the overlap years 2001–04 between the two datasets. Weekly rainfall climatologies, area-averaged over the region 70°E–85°E, 5°N–35°N, during June–September from IMD (Figure 1, blue line) and satellite data (Figure 1, red line) shows good correspondence. In view of the likely bias between the two datasets, the rainfall has been normalized to the respective maximum (Figure 1). It can be seen that the two distributions are similar, with high correlation coefficient. The corresponding comparison of the distribution of the number of events in the two datasets (normalized to the respective maximum) also shows similar distributions in the two datasets (Figure 2). Finally, an examination of intensity vs occurrence of events in the two datasets reveals similar characteristics (Figure 3); the initial sharp drop around the normalized intensity of 0.1 is followed by a

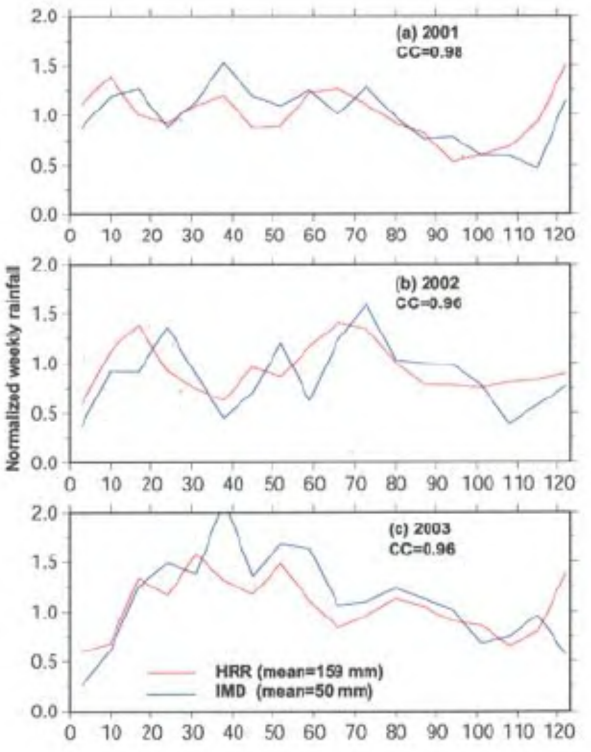


**Figure 1.** Weekly rainfall during June–September from IMD (blue line) and high resolution data (red line) for 2001 (top panel), 2002 (middle panel) and 2003 (bottom panel). The correlation coefficient between the two normalized series is given in the respective panel. Normalization has been done with respect to the three-year mean for each series, as given in bottom panel.

flat distribution (inset, Figure 3) of events at higher intensities. As expected, the maximum in the (coarse-resolution) IMD data is much lower than that in the satellite data.

We have also considered the three-hourly rainfall available on the 0.25° grid for the period 2001–06 from the Tropical Rainfall Measuring Mission (TRMM). A comparison of spatial distribution of cumulative daily rainfall (1 May 2001–31 December 2004) from IMD, TRMM and HRR (Figure 4) shows the three datasets have essentially comparable climatology. It may be noted that the IMD climatology is significantly different from the other two over Northeast India, and Jammu and Kashmir. Interestingly, however, these are also the locations over which the IMD observations are most scarce (Figure 4, bottom right). A similar conclusion holds for distribution of the number of rainy days (24-h rainfall >0.25 cm; Figure 5) and heavy-rainfall (24-h rainfall >5 cm; Figure 6) events. In particular, greater occurrence of heavy-rainfall events over the eastern coast in IMD (Figure 6), appears to be an artifact of relatively sparse observations over this area. These results show that the HRR dataset provides a reliable resource for analysing vulnerability and observation system design at the required resolution. The extreme rainfall events at a grid point were then categorized based on the 24-h accumulated rainfall.

A quantity essential for the assessment of vulnerability is the distribution of occurrence of events at a given location. We have quantified this in terms of the accumulated (2001–06) number of events with intensity greater than 25 cm/day at a given grid point. Although 25 cm is a somewhat arbitrary threshold, these events can be considered as high-impact localized events unlikely to be captured in coarse-resolution analysis. In order to quantify the degree of vulnerability, we have categorized the ERE further based on their intensity (Table 1). In addition to the category-wise analysis of the ERE, we have also examined their duration (in terms of 24-h accumulated rainfall) to assess the duration of their impact.

The spatial distribution of occurrence clearly shows the existence of certain hotspots (circled) of vulnerability (Figure 7). The circles indicate areas with annual average number of ERE exceeding 5, indicating at least one very high-impact rainfall event per year. While many of these hotspots lie over the coastal regions (Gujarat, Mumbai, Mangalore and Orissa), as expected, a significant number is also found over land, especially over North India. Over the ocean, the ERE are not uniformly distributed, but are

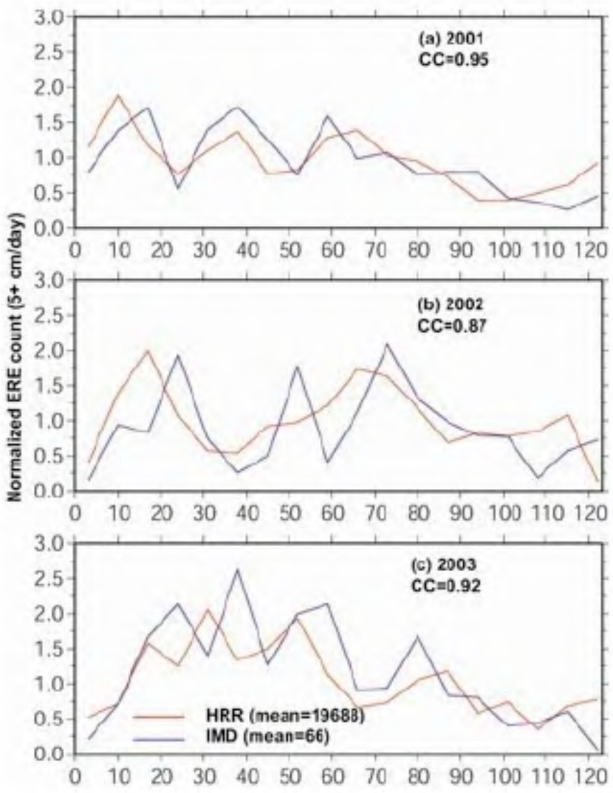


**Figure 2.** Weekly ERE counts during June to September from IMD (blue line) and high resolution data (red line) for 2001 (top panel), 2002 (middle panel) and 2003 (bottom panel). The correlation coefficient between the two normalized series is given in the respective panel. The ERE have been defined as events with 24-h accumulated rainfall at a grid exceeding 5 cm. Normalization has been done with respect to the three-year respective mean as given in the bottom panel.

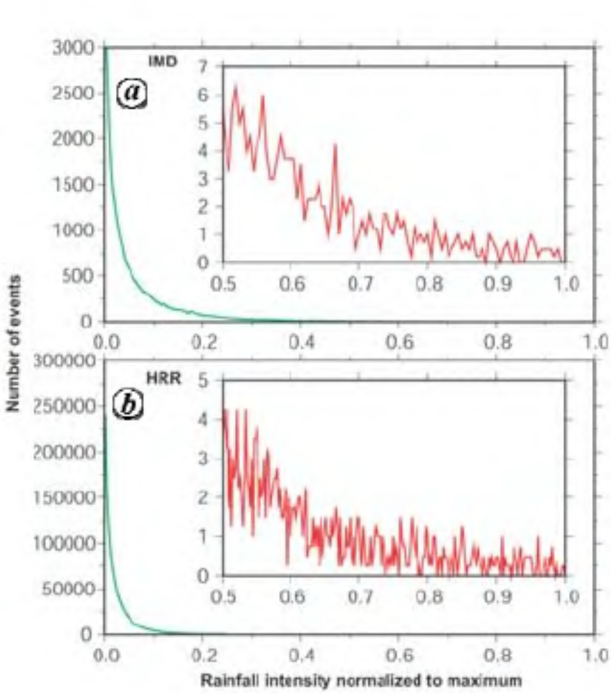


**Figure 3.** Occurrence of rainfall events of different intensities averaged over the years 2001–03. The *x*-axis represents intensity of rainfall events normalized to the respective maximum: (***a***) IMD (normalized by 20 cm) and (***b***) HRR (normalized by 50 cm). The *y*-axis shows the number of rain events in a given category during June–September over the area 70°E–85°E, 5°N–30°N.

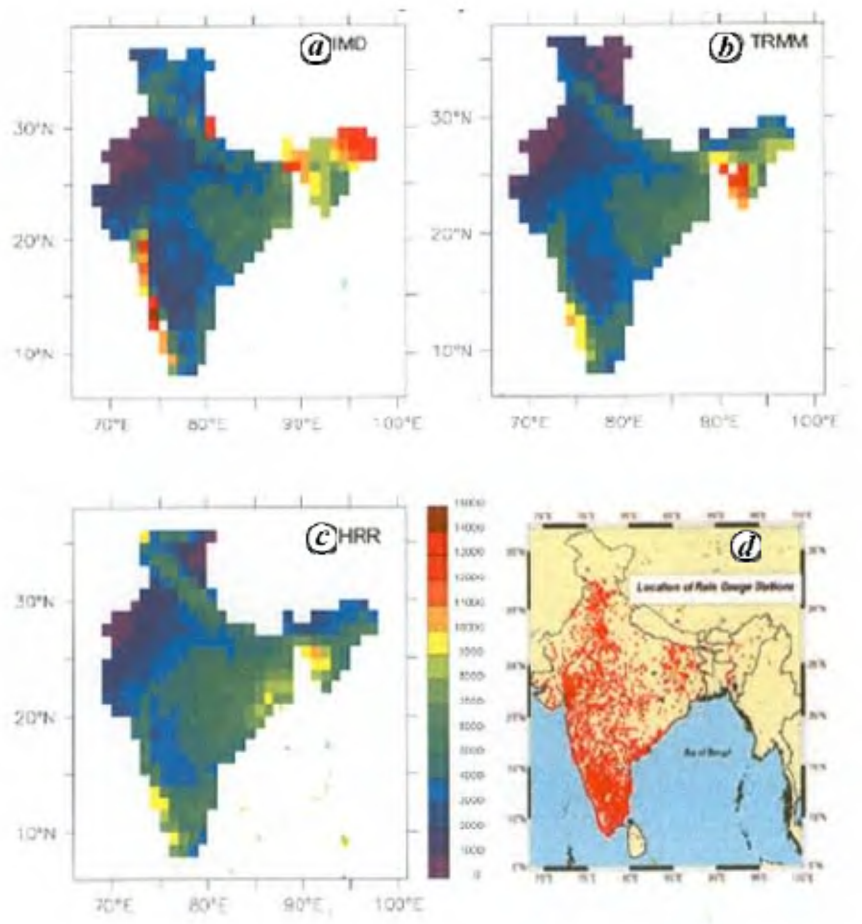


**Figure 4.** Spatial comparison of cumulative rainfall (mm) derived from daily averaged rainfall data: (***a***) IMD, (***b***) TRMM and (***c***) HRR. Both TRMM and HRR rainfall data are regridded to the IMD grid by simple averaging. The daily TRMM rainfall is derived from three-hourly data. (***d***) Location of 1803 rain gauge stations used in IMD gridded data[10].

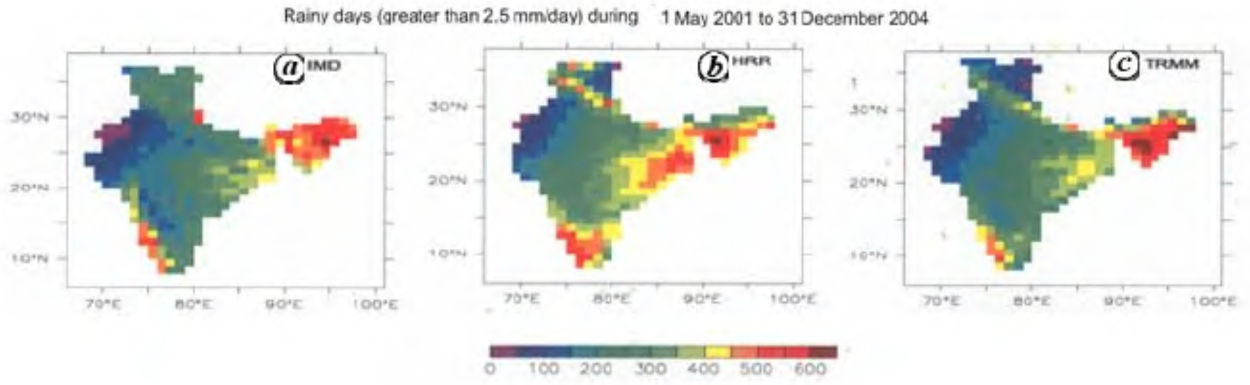


**Figure 5.** Spatial comparison of number of rainy days (>2.5 mm/day) derived from daily averaged rainfall data: (***a***) IMD, (***b***) TRMM and (***c***) HRR. Both TRMM and HRR rainfall data are regridded to the IMD grid by simple averaging. The daily TRMM rainfall is derived from three-hourly data.

clustered around island masses and the mean position of the Inter-Tropical Convergence Zone (ITCZ).

Distribution of extreme rainfall events of different intensities for different years reveals the strongly localized

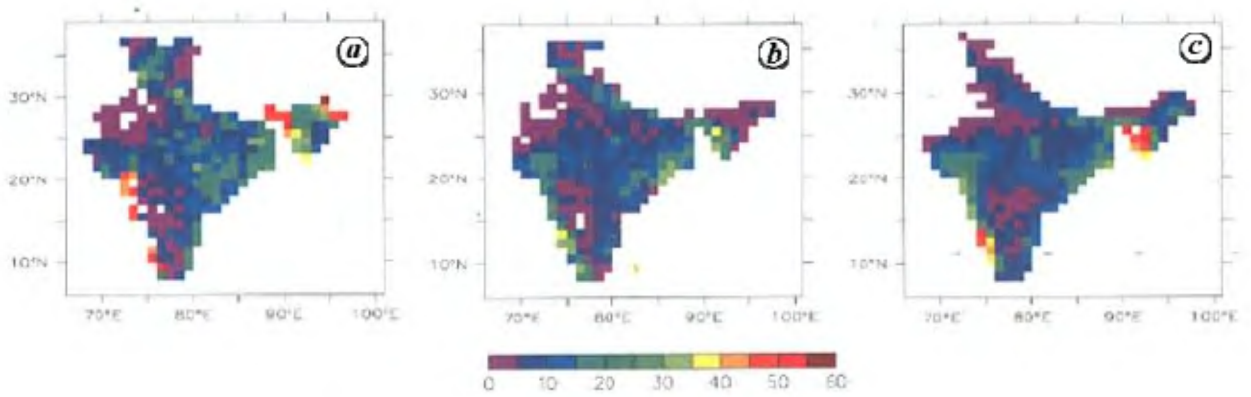


**Figure 6.** Spatial comparison of number of heavy-rainfall events (> 50 mm/day) derived from daily averaged rainfall data: (***a***) IMD, (***b***) TRMM and (***c***) HRR. Both TRMM and HRR rainfall data are regridded to the IMD grid by simple averaging. The daily TRMM rainfall is derived from three-hourly data.

**Table 1.** Interannual variation in the number of extreme rain events (JJA)

| | Number of extreme rainfall events over 70–90°E; 5–35°N for | | | | | | | |
|---|---|---|---|---|---|---|---|---|
| Category (cm/day) | 2001 | 2002 | 2003 | 2004 | 2005 | 2006 | Mean | Standard deviation |
| 25–35 | 447 | 332 | 547 | 186 | 405 | 220 | 356 | 137.94 |
| 35–45 | 86 | 81 | 57 | 55 | 75 | 24 | 63 | 22.88 |
| 45–55 | 38 | 42 | 16 | 26 | 39 | 10 | 29 | 13.32 |
| > 55 | 39 | 56 | 14 | 44 | 78 | 17 | 41 | 24.13 |
| Total | 610 | 511 | 634 | 311 | 597 | 271 | 489 | 159.39 |

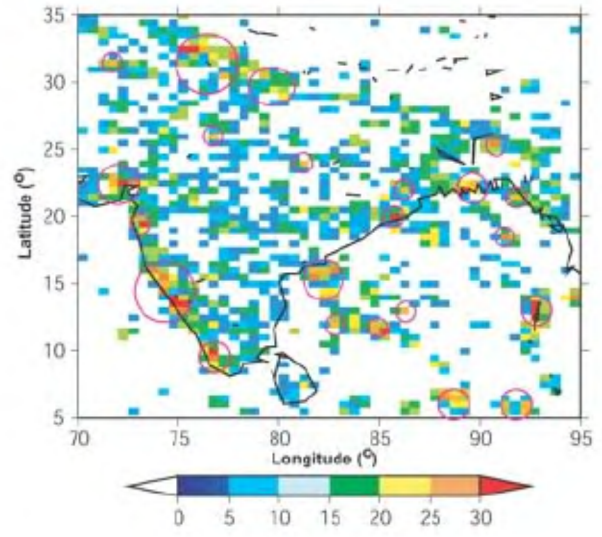


**Figure 7.** Number of different categories of EREs accumulated over five years (May 2001–August 2006) over the Indian region. Two prominent features are the relatively large number of hotspots over India and absence of events of higher intensity (more >25 cm/day) over the ocean.

nature of their occurrence (Figure 8). In fact, most ERE of intensity greater than 35 cm/day are confined to a narrow longitudinal band that extends from the west coast of India to 35°N, in a more or less continuous fashion. The south-north extent of this band, from the coastal region to the continental interior, emphasizes the relatively minor role of the oceanic environment in the genesis and evolution of these extreme events (Table 2). Further, while the oceanic region shows a large number of lower-intensity events (Table 2), it has few high-intensity events. In fact, for intensity ≤25 cm/day, the number of ERE is larger over the ocean (Table 2), as expected, with a sharp fall beyond 35 cm/day. Along with Figure 2, these results once again show that areas of high rainfall or large number of rainy days are not necessarily those of extreme rainfall events. It may be noted that (Table 2) while the number of ERE in the category ≥35 cm/day is about one-fourth that in the category ≥25 cm/day over land, this ratio is close to zero over the Bay of Bengal (BoB), the high-intensity ERE are thus rare over the BoB, even in terms of relative occurrence.

Seasonal distributions of ERE for the five years pertaining to two seasons, March–May and July–August, are shown in Figure 9. While the general pattern of distribution (Figure 8) is clearly obvious for each of the years, there is also significant interannual variability. The interannual variability of ERE, further highlighted in Table 1, shows their number for the June–August period for each category for the five years. While the average number of events per year is 489, the standard deviation is 159, al-

**Table 2.** Regional occurrence of number of extreme rainfall events

| | Number of extreme rainfall events during 2001–06 | |
|---|---|---|
| Category (cm/day) | India (74°E–83°E, 12°N–35°N) | Bay of Bengal (85°E–95°E, 5°N–17°N) |
| ≥ 0.5 | 6,282,007 | 8,940,833 |
| 15–25 | 9,959 | 23,008 |
| 25–35 | 1,187 | 898 |
| 35–45 | 383 | 8 |
| 45-55 | 162 | 0 |
| > 55 | 330 | 0 |

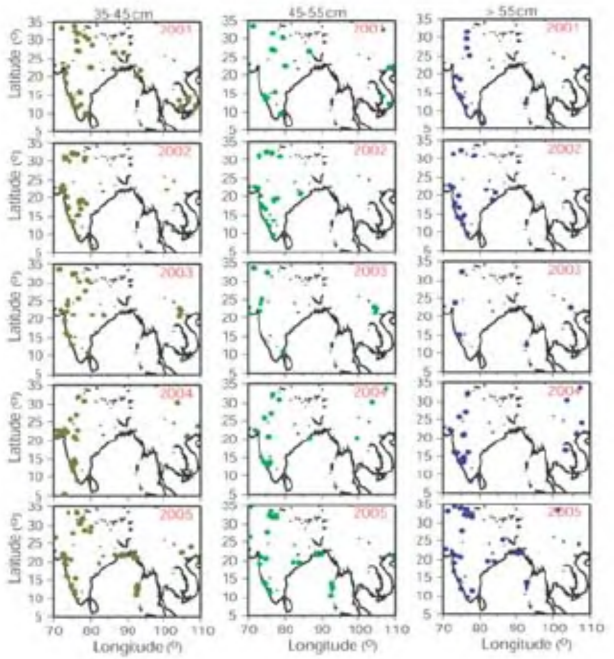


**Figure 8.** Year-wise distribution of extreme rainfall events of different intensities for June–August for five years. The left, middle and the right panels show respectively, ERE with 24-h accumulated rainfall in the range 35–45, 45–55 cm/day and more than 55 cm/day rainfall. Strong interannual variability in the number and distribution of these events is noticeable.

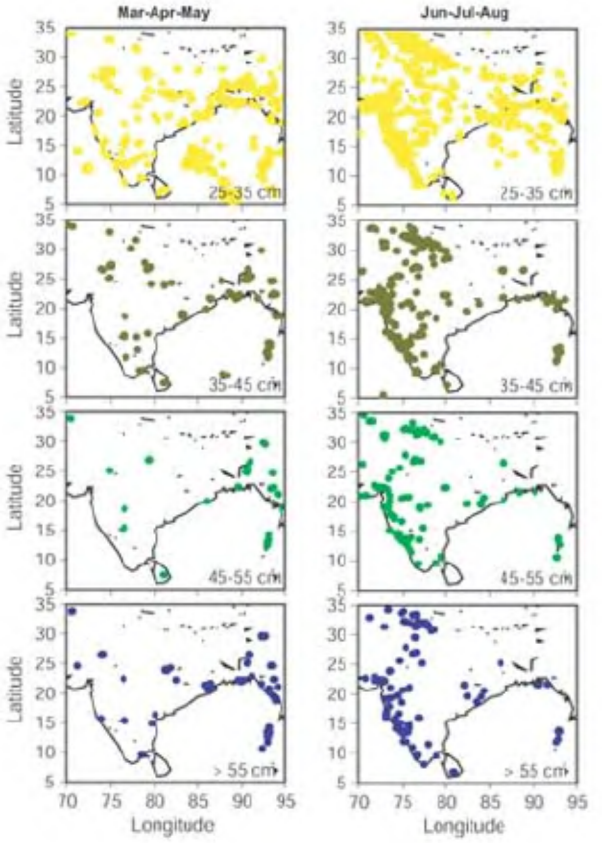


**Figure 9.** Distribution of (five-year average, 2001–06) ERE for different categories over the South Asian region. The left (right) panels represent seasonal average for March–May (June–August). Two prominent features are the conspicuous absence of high-intensity events over the ocean among both seasons, and the narrow south-north band of extreme events during June–August.

most 32.5% of the mean. While the minimum number of ERE (given by the total in Table 1) is 271 (2006), the maximum is 634 (2003); however, it is the maximum number that is critical in terms of preparedness to ERE. It may, however, be emphasized that interpretation of quantities like standard deviation for small sample size has some inherent limitations.

With respect to their lifetimes most ERE appear to be short-lived, as expected. Table 3 shows that almost all of them during the five-year period were from rainfall episodes that lasted 24 h or less (which cannot be determined from daily rainfall). Significant seasonality in the number of ERE, as seen from Figures 2 and 3, strongly suggests that the large-scale environment exerts significant control over the genesis of ERE. It has been shown that large-scale systems do have significant influence on the dynamics of small-scale systems[11,12]. There is also widespread concern regarding the weakening of Indian summer monsoon[13] and possible increase in the number and intensity of heavy-rainfall events in response to global warming[14–16]. However, strong spatio-temporal variability, especially the strong interannual variability of ERE, poses significant challenge to quantifying and ascertaining such a change. Finally, the strongly localized nature

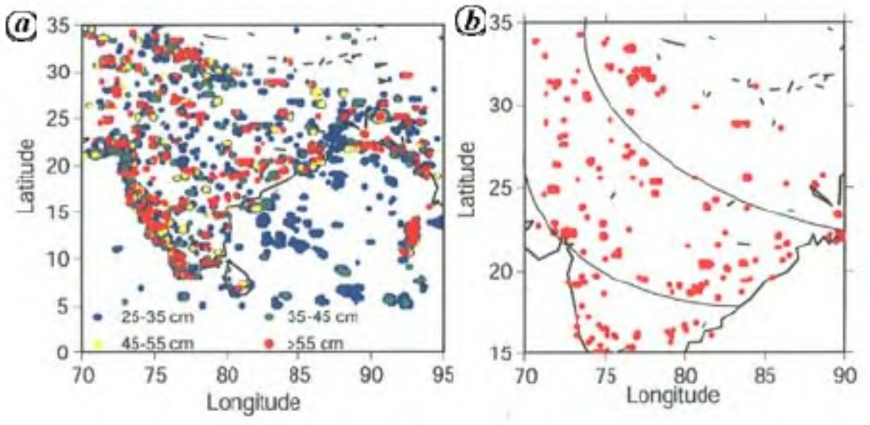


**Figure 10.** ***a***, Spatial distribution of ERE of different categories accumulated over five years (2001–05). The high density of ERE over the west coast and along the flanks of the monsoon trough is prominent. ***b***, ERE with intensity greater than 55 cm/day over the Continental Trough Convergence Zone.

**Table 3.** Lifetime of number of extreme rainfall events in different categories during May 2001–August 2006

| | Number of extreme rainfall events with duration | | |
|---|---|---|---|
| Category (cm/day) | 1 day | 2 days | 3 days |
| 25–35 | 4356 | 19 | 0 |
| 35-45 | 1080 | 4 | 1 |
| 45–55 | 469 | 1 | 0 |
| > 55 | 823 | 5 | 0 |

of the ERE hotspots indicates the need for horizontal resolution far beyond what is employed today, especially in global and climate simulations.

The highly localized nature of ERE as revealed by our analysis highlights the importance of sufficiently high resolution for simulation of these events. A dataset like the NCEP Reanalysis[9] with a horizontal resolution of about 250 km, or the daily gridded rainfall at about 110 km recently prepared by IMD[10], for example, cannot adequately represent the distribution and degree of vulnerability to these high-impact events.

An important application of such high-resolution analysis can be in the area of precision observation design. From Figure 10 *a*, we note that the distribution of ERE clearly marks the corridor of the monsoon trough (Continental Tropical Convergence Zone, CTCZ) over the Indo-Gangetic Plane, in the same way that the (lower intensity) ERE mark the mean position of the ITCZ over the ocean. To bring out the ERE-structure of the CTCZ more clearly, we show in Figure 10 *b*, only events in the category of daily rainfall ≥55 cm/day over 15°N–35°N and 70°E–90°E. The CTCZ, as represented by ERE, reveals interesting fine structures. In particular, ERE of highest intensities are not found deep inside the corridor, but are distributed in a flower-pot pattern along the flanks of the CTCZ. This pattern is dynamically consistent, as the sharpest pressure gradients (and hence the strongest convergence and secondary circulation) are expected to be found along the line that separates the low-pressure trough from the surrounding area. Our analysis, however, marks this corridor and the flanks with a precision hitherto unachievable; as such, these analyses can be important inputs for precision (10 km-resolution) design of field experiments, for example, the CTCZ field experiment currently being planned in terms of location of observation platforms, or the STORM field experiments over eastern and the north-eastern India[17]. A comparison of Figure 4 *a* and *b* also hints at two main sources of ERE: the orographic ones distributed over the Western Ghats and the foothills of Himalayas, and others due to the CTCZ.

Although the impact of greater occurrence of ERE may not yet be felt over some of the non-urban locations, they represent areas of potential disaster if unplanned urbanization or industrialization is allowed. One potential application of our analysis is, therefore, in urban and industrial planning; as the ERE-prone areas are identified to a precision of 0 km, practical planning to avoid high-vulnerability areas is possible.

Although the NOAA dataset used here allows much more precise and accurate assessment of spatial and temporal distribution of ERE and thus the associated degree of vulnerability, a more comprehensive analysis requires collocated measurements of other dynamical, surface and sub-surface parameters. Based on the precision distribution of ERE revealed by our analysis, such measurements can be made by placing Automated Weather Stations (meteorological towers) over these locations. Such measurements, supplemented by other observation platforms like remote sensing and upper-air soundings, can allow analysis and forecasting of these high-impact events at precision and resolution that can be effective in applications like pro-active disaster management.

In terms of vulnerability assessment and disaster management, however, rainfall amount (or category) is only one of the (critical) inputs. The forecast of rainfall needs

to be integrated, with appropriate weight for reliability of the forecast, with models of impact and logistics which require detailed information on infrastructure, population and other parameters over the location. Such models, which are necessarily location-specific, are in their infancy, especially in India.


1. James, M. K., Urban metabolism and disaster vulnerability in an era. In *Earth System Analysis* (eds Schellnhuber, H.-J. and Wenzel, V.), Springer-Verlag, Berlin, 1998, pp. 359–377.
2. Gilbet, A. and Gugler, J., *Cities, Poverty and Development: Urbanization in the Third World*, Oxford University Press, Oxford, 1992.
3. Jones, B. and Kandell, W. A., Population growth, urbanization, disaster risk and vulnerability in metropolitan areas: A conceptual framework. In *Environmental Management and Urban Vulnerability* (eds Kreimer, A. and Munasinghe, M.), World Bank Discussion Paper 168, 1992, pp. 51–76.
4. De, U. S., Dube, R. K. and Prakasa Rao, G. S., Extreme weather events over India in the last 100 years. *J. Indian Geophys. Union*, 2005, **9**, 173–187.
5. Haylock, M. and Nicholas, N., Trends in extreme rainfall indices for an updated high quality data set for Australia, 1910–1998. *Int. J. Climatol.*, 2000, **20**, 1533–1541.
6. Parker, M. D. and Johnson, R. H., Organizational modes of midlatitude mesoscale convective systems. *Mon. Weather Rev.*, 2000, **128**, 3413–3435.
7. Xie, P. and Arkin, P. A., Analyses of global monthly precipitation using gauge observations, satellite estimates and numerical model predictions. *J. Climate*, 1996, **9**, 840–858.
8. Pingping, X., Yarosh, Y., Love, T., Janowaik, J. E. and Arkin, P. A., A real-time precipitation analysis over South Asia. AMS Meeting, USA, 2002, 3.15–3.16.
9. Kisstler, R. *et al.*, The NCEP–NCAR 50-year Reanalysis: Monthly means CD-ROM and documentation. *Bull. Am. Meteorol. Soc.*, 2001, **82**, 247–267.
10. Rajeevan, M., Bhate, J., Kale, J. D. and Lal, B., Development of high resolution daily gridded rainfall data for the Indian region, India Meteorological Department. *Meteorol. Monograph Climatology*, 22/2005, 1–26.
11. Tamguay, M., Bartello, P. and Gauthier, P., Four dimensional data assimilation with a wide range of scales. *Tellus B*, 1995, **47**, 974–997.
12. Goswami, P. and Patra, G. K., Characteristic scale of convective organization and monsoon intensity. *Geophys. Res. Lett.*, 2004, **31**, L24109.
13. Ramesh, K. V. and Goswami, P., Reduction in temporal and spatial extent of the Indian summer monsoon. *Geophys. Res. Lett.*, 2007, **34**, L23704.
14. Palmer, T. N. and Raisanen, J., Quantifying the risk of extreme seasonal precipitation events in a changing climate. *Nature*, 2002, **415**, 512–514.
15. Schnur, R., The investment forecast. *Nature*, 2002, **415**, 483–484.
16. James, M. K. and Ericksen, N., Effects of climate changes on weather-related disasters. In *Confronting Climate Change: Risks, Implications and Responses* (ed. Mintzer, I.), Cambridge University Press, Cambridge. 1992, pp 141–152.
17. Mohanty, U. C. *et al.*, Weather summary during pilot experiment of severe thunderstorms – Observations and regional modelling (STORM), DST Report, 2006, pp. 1–146.


ACKNOWLEDGEMENTS. We thank Pingping Xie, NOAA/Climate Prediction Centre, USA for providing information about the high-resolution satellite-derived rainfall data over the South Asian region. This work was partially supported by a research grant from CSIR, New Delhi.

Received 20 March 2007; revised accepted 10 March 2008

# Impact of ice-albedo feedback on hemispheric scale sea-ice melting rates in the Antarctic using Multi-frequency Scanning Microwave Radiometer data

**Amitabh Mitra[1], I. M. L. Das[1,2,*], Mihir Kumar Dash[3], S. M. Bhandari[4] and N. K. Vyas[4]**

[1]K. Banerjee Centre of Atmospheric and Ocean Studies,
[2]Department of Physics, University of Allahabad,
Allahabad 211 002, India
[3]Centre for Oceans, Rivers, Atmosphere and Land Sciences,
Indian Institute of Technology, Kharagpur 721 302, India
[4]Space Applications Centre, Indian Space Research Organization,
Ahmedabad 380 015, India

**The sea-ice cover in the polar regions is one of the most expansive and seasonal geophysical parameters on the earth's surface. The presence or absence of sea-ice affects the atmosphere and the ocean, and therefore the climate in many ways. In this study we have used the Multi-frequency Scanning Microwave Radiometer (MSMR) brightness temperature data over the Antarctic/Southern Ocean region to calculate the weekly sea-ice extents, during the melting phase from August 1999 to March 2000 to quantitatively estimate the melting rates of sea-ice on a hemispheric scale. Compared to the melting rates based on the seasonal cycle of the solar irradiance, the MSMR-estimated melting rate remains less until the beginning of October and then rapidly increases to its peak value by the end of December. The observed melting rate behaviour indicates that apart from the seasonal cycle of solar irradiance, it is controlled by other mechanisms like the ice-albedo feedback. The present study estimates the feedback factor, response time and acceleration in the melting rate, which are important towards a better quantitative understanding of the future of Antarctic sea-ice variability, and the climate trends in the context of global warming.**

**Keywords:** Hemispheric scale, ice-albedo feedback, melting rate, sea-ice extent.

IN the polar regions, sea water freezes at the surface due to the seasonal cycle of insolation producing a thin and discontinuous blanket of ice called sea-ice, having thickness of less than a few metres. The sea-ice acts as an efficient barrier to the free exchange of heat, moisture, and momentum fluxes between the ocean and the atmosphere, substantially altering the radiative and turbulent components of the surface-heat balance. Since the sea-ice layer is thin, its areal extent and thickness respond rapidly to changes in the surface heat balance and modulate the in-

*For correspondence. (e-mail: profimldas@yahoo.com)